

Functional connectivity for the language network in the developing brain: 30 weeks of gestation to 30 months of age

Dustin Scheinost^{1,2,3,4}, Joseph Chang³, Cheryl Lacadie¹, Emma Brennan-Wydra⁴, R. Todd Constable^{1,2,5}, Katarzyna Chawarska^{3,4,6,†}, Laura R. Ment^{6,7,†}

¹Department of Radiology & Biomedical Imaging, Yale School of Medicine, New Haven, CT 06510, USA,

²Department of Biomedical Engineering, Yale University, New Haven, CT 06520, USA,

³Department of Statistics & Data Science, Yale University, New Haven, CT 06520, USA,

⁴Child Study Center, Yale School of Medicine, New Haven, CT 06510, USA,

⁵Department of Neurosurgery, Yale School of Medicine, New Haven, CT 06510, USA,

⁶Department of Pediatrics, Yale School of Medicine, New Haven, CT 06510, USA,

⁷Department of Neurology, Yale School of Medicine, New Haven, CT 06510, USA

*Address correspondence to Dustin Scheinost, PhD, Magnetic Resonance Research Center, 300 Cedar St, P.O. Box 208043, New Haven, CT 06520-8043, USA. Email: dustin.scheinost@yale.edu

†Katarzyna Chawarska and Laura R. Ment have contributed equally to the manuscript

Although the neural scaffolding for language is putatively present before birth, the maturation of functional connections among the key nodes of the language network, Broca's and Wernicke's areas, is less known. We leveraged longitudinal and cross-sectional data from three sites collected through six studies to track the development of functional circuits between Broca's and Wernicke's areas from 30 weeks of gestation through 30 months of age in 127 unique participants. Using resting-state fMRI data, functional connectivity was calculated as the correlation between fMRI time courses from pairs of regions, defined as Broca's and Wernicke's in both hemispheres. The primary analysis evaluated 23 individuals longitudinally imaged from 30 weeks postmenstrual age (fetal) through the first postnatal month (neonatal). A secondary analysis in 127 individuals extended these curves into older infants and toddlers. These data demonstrated significant growth of interhemispheric connections including left Broca's and its homolog and left Wernicke's and its homolog from 30 weeks of gestation through the first postnatal month. In contrast, intrahemispheric connections did not show significant increases across this period. These data represent an important baseline for language systems in the developing brain against which to compare those neurobehavioral disorders with the potential fetal onset of disease.

Key words: fetal; infant; neonate; perinatal transition; trajectory.

Introduction

Language is critical to human development. In the brain, the canonical language network is anchored in two key regions: Broca's area, located in the left inferior frontal gyrus, and Wernicke's area in the left superior temporal gyrus, and each of these have homologs in the right hemisphere. Wernicke's area subserves receptive language, while expressive language is localized to Broca's area. Once developed, the language network is characterized by strong functional connectivity between all pairwise connections for these two regions and their right hemisphere homologs (Tomasi and Volkow 2012), but the earliest developmental trajectories of these connections remains to be fully characterized.

The functional connectivity scaffolding for Broca's and Wernicke's begins developing prior to birth

(Jardri et al. 2012; Thomason et al. 2013). Cross-sectional fetal functional connectivity data show that interhemispheric connectivity, including the inferior frontal gyrus and medial temporal gyrus, increases across the third trimester of gestation (Thomason et al. 2013), and intrahemispheric networks encompassing these regions become more left-lateralized across the third trimester (Thomason et al. 2014). Together, these data suggest these key features of the fetal functional connectome for language foreshadow that in older individuals but do not characterize that critical interval from the intra-uterine to extra-uterine environment (Turk et al. 2019).

After birth, the maturation of the functional connections of Broca's and Wernicke's areas continues. Neonates show strong interhemispheric connectivity between both left Broca's and Wernicke's areas and

Received: July 31, 2021. Revised: September 20, 2021. Accepted: October 12, 2021

© The Author(s) 2021. Published by Oxford University Press. All rights reserved. For permissions, please e-mail: journals.permission@oup.com.

This is an Open Access article distributed under the terms of the Creative Commons Attribution Non-Commercial License (<https://creativecommons.org/licenses/by-nc/4.0/>), which permits non-commercial re-use, distribution, and reproduction in any medium, provided the original work is properly cited. For commercial re-use, please contact journals.permissions@oup.com

their right hemisphere homologs (Perani et al. 2011; Kwon et al. 2015; Emerson et al. 2016). Notably, neonates demonstrated an analogue of the adult network for language, which showed no effect of age from 37.5–44 weeks postmenstrual age (PMA) (Eyre et al. 2021). In contrast, intrahemispheric connections between Wernicke's and Broca's are only weakly present at birth (Perani et al. 2011; Emerson et al. 2016) and may not fully develop until toddlerhood (Emerson et al. 2016). Overall, the functional connectivity patterns for Wernicke's and Broca's become more refined in parallel with the refinement of receptive and expressive skills in postnatal life (Bruchhage et al. 2020).

Nevertheless, the transition from a fetus to a neonate is physiologically significant for the developing brain (Morton and Brodsky 2016; Schwaberg et al. 2018). Current studies have focused solely on prenatal or postnatal development of Broca's and Wernicke's connectivity, with critical longitudinal trajectories from the third trimester of gestation through the perinatal transition and the first postnatal month missing from the literature. Using cross-sectional and longitudinal data from multiple datasets, we addressed this gap in knowledge and interrogated the development of functional connectivity between Broca's and Wernicke's areas and their homologs from 30 weeks of gestation through 30 months of age in typically developing fetuses, infants, and toddlers. Since prior fMRI and neuropathologic studies demonstrated lateralization for language (Dehaene-Lambertz et al. 2002; Dehaene-Lambertz et al. 2006) and differential development of interhemispheric connectivity (Huttenlocher and Dabholkar 1997), secondary hypotheses compared the trajectories of both intra- and interhemispheric language networks. The primary analysis interrogated language connectivity of 23 individuals longitudinally imaged at 2–3 time points from the third trimester through the first postnatal month. A secondary analysis included 127 individuals with cross-sectional and longitudinal data from third trimester through 30 months of age.

To the best of our knowledge, our results suggest for the first time that interhemispheric functional connectivity of the language network develops rapidly across the third trimester of gestation through the first postnatal month with significant interhemispheric connectivity observable in the perinatal period. In contrast, we report weak intrahemispheric connectivity through the 30th postnatal month. These data provide important information about the functional organization in the developing brain and provide a baseline against which to compare disorders characterized by fetal onset of diseases affecting the connectome (Scheinost, Kwon, Lacadie, et al. 2016a; Thomason et al. 2017; Peyvandi et al. 2021).

Methods

This work includes both longitudinal and cross-sectional imaging data from four studies collected at the Yale

School of Medicine as well as two open-source datasets obtained from the National Institute of Mental Health Data Archive (NDA): 1) the Cincinnati MR Imaging of Neurodevelopment study (C-MIND; dataset identifier: NDARCOL0002329) and 2) the University of California Los Angeles Autism Center of Excellence project (UCLA; dataset identifier: NDARCOL0002026). Studies at the Yale School of Medicine were approved by the Yale University Institutional Review Board; all parent(s) provided written consent. The C-MIND and UCLA studies were reviewed and approved by the original investigators' Institutional Review Boards, and signed written informed parental consent was obtained by the original study investigators. The two Yale studies that consist of longitudinal fetal-to-neonatal imaging (labeled Fetal-neonatal Cohort #1 and Fetal-neonatal Cohort #2, respectively) were used for the primary and secondary analyses. These two cohorts were scanned on different scanners. The C-MIND study, the UCLA study, and the two Yale studies with only neonatal imaging (labeled Neonatal Cohort #1 and Neonatal Cohort #2, respectively) were used for secondary analyses only. An overview of composition of the study cohorts is presented in Table 1.

Participants

Fetal-neonatal Cohort #1: This cohort consists of longitudinal data from the third trimester to the neonatal period collected as part of the Yale Autism Center of Excellence Program Project. Between 9 April 2018 and 11 March 2020, 16 pregnant women were recruited for scanning at 30–33 weeks and 34–36 weeks PMA. Mothers who participated in the fetal scans were invited to have their infants participate in the neonatal functional connectivity protocol. Usable longitudinal data were available for 13 of the 16 maternal–infant dyads with at least two scans per participant. Inclusion criteria for fetuses included pregnant women with no family history of autism spectrum disorder (ASD) who met the following criteria: 1) 26–28 weeks gestational age; 2) estimated fetal weight, femur length and bi-parietal diameter appropriate for gestational age; 3) no known chromosome or structural abnormalities; 4) no brain injury on clinical ultrasound; 5) no congenital infections; 6) no known ethanol exposure since confirmation of pregnancy; 7) no known tobacco/nicotine use since confirmation of pregnancy; 8) no known illicit drug use/abuse; 9) singleton pregnancy; 10) receiving regular prenatal care; 11) maternal age 21–35 years; 12) no morbid obesity; and 13) mother able to give permission. Exclusion criteria included 1) any contraindications for MRI scanning; 2) too large to fit in the MRI machine comfortably for 45 minutes; 3) a clinically ordered MRI scheduled in the future; 4) difficulty lying down and remaining still for 45–60 minutes; 5) current drug, alcohol and/or tobacco/nicotine use; and 6) preterm birth (for neonates). Drug screening (Integrated E-Z Split Key Cup II, Alere San Diego, Inc, San Diego, CA 92121) and alcohol and tobacco screening tools were administered to all mothers at the time of each fetal MRI study using the

Table 1. Composition of the study cohorts

Cohort	Unique individuals	Individuals with usable longitudinal data ^a	Ages scanned	Number of usable scans	Analyses
Fetal-neonatal Cohort #1	16	13	30–33 wks PMA 34–36 wks PMA < 1 mo	14 12 11	Primary+ Secondary
Fetal-neonatal Cohort #2	11	10	30–33 wks PMA 34–36 wks PMA < 1 mo	10 9 8	Primary+ Secondary
Neonatal Cohort #1	25	0	< 1 mo	23	Secondary only
Neonatal Cohort #2	12	0	0.4–1.5 mo	12	Secondary only
UCLA	34	16	1–2 mo 9 mo	25 27	Secondary only
C-MIND	31	5	1–35 months	36	Secondary only

^aLongitudinal data are defined as usable data at more than 1 time point.

Fagerstrom Test for Nicotine Dependence and the Alcohol Timeline Followback assessments (Sobell and Sobell 1995; Weinberger et al. 2007). Participants included in the present analysis had no familial history of autism spectrum disorder (ASD) (Table 1).

Fetal-neonatal Cohort #2: This cohort consists of longitudinal data from the third trimester to the neonatal period. Eleven women and their infants participated in a similar longitudinal protocol as above and were recruited between May 2015 and September 2016. Inclusion and exclusion criteria were as in *Fetal-neonatal Cohort #1*. Usable longitudinal data are available for 10 of the 11 mother-infant dyads. Mothers were screened for drug, alcohol, and tobacco use according to standard protocol at each prenatal clinical visit.

Neonatal Cohort #1: Twenty-three healthy term neonates, born between 37 and 41 weeks PMA were included in this study (Kwon et al. 2014). Scans were completed between 1 September 2010 and 31 October 2013. Inclusion criteria for neonates included singleton pregnancy, term birth, and appropriate for gestational age. Exclusion criteria included evidence of congenital infections, congenital malformations, chromosomal disorders, seizures, and/or contraindications to MRI. Drug and alcohol screening data are not available for this cohort.

Neonatal Cohort #2: Twelve healthy term infants born between 37- and 41-weeks PMA were scanned within the first 6 weeks of life as part of their participation in the Yale Autism Center of Excellence Program Project. The scans were completed between 11 April 2018 and 5 November 2020. As in the *Neonatal Cohort #1*, inclusion criteria included singleton pregnancy, term birth, and appropriate for gestational age. Similarly as with the *Neonatal Cohort #1*, exclusion criteria included: 1) congenital infections; 2) non-febrile seizure disorder; 3) hearing loss; 4) visual impairment; 5) the presence of any known chromosomal abnormality; 6) prenatal exposure to illicit drugs; 7) major psychotic disorder in first degree relatives; and 8) contraindications to MRI including non-removable metal medical implants (i.e., patent ductus arteriosus clip). Similar to *Fetal Cohort #1*, only low-risk infants with no family history of autism or other neurodevelopmental disorders are included in this analysis ($n = 12$).

UCLA: Thirty-four infants were included from this dataset. Inclusion criteria included 1) healthy full-term infant with no perinatal complications; and 2) >3000 g birth weight. Exclusionary criteria included the following: 1) genetic syndromes or neurological conditions; 2) chronic medical conditions or significant perinatal insult impacting development; 3) severe visual, hearing, or motor impairment; 4) non-English speaking families; and 5) contraindication for MRI. As the data were deidentified, specific scan dates were not available. Drug, alcohol, and tobacco screening data are not available for the UCLA cohort. As the UCLA study included infants with both high- and low-risk for developing ASD, only low-risk infants with no family history or other neurodevelopmental disorders are included in this analysis ($n = 34$). Nineteen of the infants scanned at 1–2 months underwent repeat studies at 9 months of age.

C-MIND: The C-MIND study includes data from 31 typically developing children scanned between 1 month and 3 years with 28 children being scanned at over 9 months. As the data were deidentified, specific scan dates were not available. Exclusion criteria included 1) PMA ≤ 37 weeks or ≥ 42 weeks; 2) birth weight < 10% for gestational age (i.e., small for gestational age); 3) history of head trauma with loss of consciousness; 4) special education; 5) orthodontic braces or other metallic implants; and 6) standard MRI compatibility indications. Drug, alcohol, and tobacco screening data are also not available for the C-MIND cohort. Five of the individuals scanned in the C-MIND study have longitudinal imaging.

Imaging Parameters

Fetal-neonatal Cohort #1: All MRIs were performed in the natural, unmedicated state. Fetuses were studied using repeat MRI protocols completed in <60 minutes using a 3 Tesla Siemens (Erlangen, Germany) Prisma MR system and a flexible, lightweight (~1 lb), cardiac 32-channel body coil. Five functional runs were acquired (TR = 2000 ms, TE = 30 ms, FoV = 352 × 400 mm, flip angle 90°, matrix size 88 × 100, SAR < 0.4, slice thickness 3 mm, Bandwidth = 2940 Hz/pixel, 32 slices). Each of the 5 functional runs were comprised of 150 volumes (5 minutes). All participants had at least

5 minutes of usable data. Follow-up neonatal MRI in this cohort occurred as part of a natural-sleep “feed and wrap” protocol (Kwon et al. 2014). Infants were fed, bundled with multiple levels of ear protection, and immobilized in an MRI-safe vacuum swaddler. Heart rate and O₂ saturation were continuously monitored during all scans. The same 3 Tesla Siemens (Erlangen, Germany) Skyra MR system that was employed for fetal imaging was also used for the neonatal data. Functional images were collected using an echo-planar image gradient echo pulse sequence (TR=1000 ms, TE=31 ms, FoV=184 mm, matrix size=92 × 92, slice thickness=2 mm, flip angle=62°, bandwidth=1810 Hz/pixel, 60 slices). Functional runs consisted of 360 volumes (6 minutes).

Fetal-neonatal Cohort #2: All MRIs were performed in the natural, unmedicated state. Fetuses were studied using repeat MRI protocols completed in < 60 minutes using a 3 Tesla Siemens (Erlangen, Germany) Skyra MR system and a flexible, lightweight (~1 lb), cardiac 32-channel body coil. Five functional runs were acquired (TR=1950 ms, TE=21 ms, FoV=320 mm, flip angle 90°, matrix size 94 × 94, SAR < 0.4, slice thickness 3 mm, bandwidth=2215 Hz/pixel, 32 slices). Each of the 5 functional runs were comprised of 180 volumes (5.85 minutes). On average, 291 frames (range: 176–390 frames) were retained for analysis, or greater than 9 minutes data per participant. As in fetal-neonatal Cohort #1, follow-up neonatal MRI in this cohort occurred as part of a natural-sleep “feed and wrap” protocol (Kwon et al. 2014). Infants were fed, bundled with multiple levels of ear protection, and immobilized in an MRI-safe vacuum swaddler. Heart rate and O₂ saturation were continuously monitored during all scans. The same 3 Tesla Siemens (Erlangen, Germany) Skyra MR system that was employed for fetal imaging was also used for the neonatal data. Functional images were collected using an echo-planar image gradient echo pulse sequence (TR=2120 ms, TE=22 ms, FoV=260 mm, matrix size=102 × 102, slice thickness=3 mm, flip angle=90°, bandwidth=2335 Hz/pixel, 32 slices). Functional runs consisted of 175 volumes (6.18 minutes).

Neonatal Cohort #1: Participants were scanned without sedation using the same feed-and-wrap protocol as above in a 3 Tesla Siemens (Erlangen, Germany) TIM Trio MR system with a 32-channel parallel receiver head coil. Functional images were collected using an echo-planar image gradient echo pulse sequence (TR=1500 ms, TE=27 ms, FoV=220 mm, matrix size=64 × 64, slice thickness=4 mm, flip angle=60°, bandwidth=2520 Hz/pixel, 25 slices). Functional runs consisted of 186 volumes (approximately 5 min scan length) after the first 6 volumes were removed to allow the magnetization to reach the steady state. All neonates had on average 10.7 min (SD=3) of usable functional data.

Neonatal Cohort #2: Imaging was performed on a 3 Tesla Siemens (Erlangen, Germany) Prisma MR system using a 32-channel parallel receiver head coil and the

same “feed and wrap” protocol as above. Functional runs were acquired using a multiband T2*-sensitive gradient-recalled, single-shot echo-planar imaging pulse sequence (TR=1 s, TE=31 ms, FoV=185 mm, flip angle 62°, multiband=4, matrix size 92 × 92). Each volume consisted of 60 slices parallel to the bi-commissural plane (slice thickness 2 mm, no gap). We collected 5 functional runs, each comprised of 360 volumes. Each neonate had on average 11.6 min (SD=1.4) of usable functional data.

UCLA: Imaging data were collected at ages 1–2 and 9–10 months on a 3 Tesla Siemens (Erlangen, Germany) Tim Trio scanner using a 12-channel head coil during natural sleep. Acquisition parameters were as follows, TR/TE=2000, 28 ms, flip angle=90°, FOV 192 mm, 56 × 56 matrix, 34 axial 4 mm slices, 240 volumes; scan time 8 minutes. Each infant had on average 7.6 min (SD=0.9) of usable functional data.

C-MIND: Participants, whose data are included in this analysis, were scanned during natural sleep on either a Philips 3 T Achieva system or a 3 T Siemens Magnetom Tim Trio scanner and a 32-channel head coil. Echo-planar fMRI scan parameters between the two scanners were homogenized to minimize systematic variation in the data. TR/TE=2000/35 ms, FOV=24 × 24 cm, matrix=80 × 80, and slice thickness=4 mm, yielding a spatial resolution of 3 × 3 × 4 mm. Thirty-six slices were acquired to cover the entire brain, and 140 whole-brain volumes were acquired. The scan executed a “dummy scan” interval consisting of 2 TR periods for which scans were not recorded prior to acquisition of the functional imaging data. Further, the first acquired image was also discarded during post-processing to insure image contrast at relaxation equilibrium. Total scan time for the acquisition was 5 min 8 s; each individual had on average 4.6 min (SD=0.7) of usable functional data.

Image Processing

Fetal connectivity preprocessing: Functional data were processed using validated fetal fMRI pipelines (Scheinost et al. 2018; Rutherford et al. 2021). Functional data were corrected for motion using a two-pass registration approach optimized for fetuses to correct for large and small head movements (Scheinost et al. 2018). Outlying frames were censored for data quality based on signal-to-noise ratio within the fetal brain, the final weighted correlation value from optimization, and the frame-to-frame motion between adjacent frames. These frames were defined as frame with SNR, registration quality, or motion greater/less than one standard deviation above/below the mean values over all runs.

As outlined in Thomason et al. (Thomason et al. 2017), several covariates of no interest were regressed from the data including linear and quadratic drifts, 6 motion parameters, mean cerebral-spinal-fluid (CSF) signal, mean white-matter signal, and mean gray matter signal. The data were temporally smoothed with a zero mean unit variance Gaussian filter (approximate cutoff

frequency=0.12 Hz). A gray-matter mask defined in template space was applied to the data, so only gray matter voxels were used in further calculations.

Next, to warp the language seeds from MNI space to fMRI space, a series of non-linear registrations were calculated independently and combined into a single transform. This single transformation allows the seeds to be transformed to single participant space with only one transformation, reducing interpolation error. First, the mean functional image from the motion corrected fMRI data was registered to an age-appropriate template (i.e., 31 weeks or 34 weeks gestation) (Gholipour et al. 2017) using a low-resolution non-linear registration. The fetal template was non-linearly registered to a custom infant template and this infant template was non-linearly registered to MNI space (see below for details).

Infant and toddler connectivity preprocessing: Functional data for infants and toddlers from the Yale, UCLA, and C-MIND samples were processed using an identical previously validated pipeline (Kwon et al. 2014). Functional images were slice-time and motion corrected using SPM8. Next, images were iteratively smoothed until the smoothness of any image had a full-width half-maximum of approximately 6 mm using AFNI's 3dBlurToFWHM. This iterative smoothing reduces motion-related confounds (Scheinost et al. 2014). All further analyses were performed using BioImage Suite (Joshi et al. 2011) unless otherwise specified. Several covariates of no interest were regressed from the data including linear and quadratic drifts, mean cerebral-spinal-fluid (CSF) signal, mean white-matter signal, and mean gray matter signal. For additional control of possible motion-related confounds, a 24-parameter motion model (including six rigid-body motion parameters, six temporal derivatives, and these terms squared) was regressed from the data. The data were temporally smoothed with a Gaussian filter (approximate cutoff frequency=0.12 Hz). A canonical gray matter mask defined in common space was applied to the data, so only voxels in the gray matter were used in further calculations.

Next, to warp the language seeds from MNI space to fMRI space, a series of non-linear registrations were calculated independently and combined into a single transformation. First, the mean functional image from the motion corrected fMRI data was registered to a custom infant template (as in (Scheinost, Kwon, Shen, et al. 2016b)) using a previously validated algorithm (Scheinost et al. 2017). Similarly, the infant template was registered to the MNI brain using the same algorithm.

Seed connectivity: After the four canonical language seeds (L Broca's and Wernicke's and their right hemisphere homologs; see Table S1 for network node coordinates) were warped into single participant space, the time course for each of these regions was then computed as the average time course across all voxels in the reference region. The time courses were correlated between Broca's and Wernicke's areas and their homologs. Each

correlation was transformed to z-values using Fisher's transform, resulting in four functional connections per individual. Connectivity strength for the overall language network was defined as the average of these four connections.

Head Motion: Since head motion can potentially confound functional connectivity, we included several steps to ensure adequate control of motion confounds. For fetuses, we strictly censored all data for motion and data quality. There were no group differences in motion between the two fetal timepoints (Table S2). For infants and toddlers, the mean frame-to-frame displacement was calculated for each run for every individual. Runs with a mean frame-to-frame displacement greater than 0.2 mm were removed from further analysis. Additionally, iterative smoothing and regression of 24 motion parameters (6 rigid-body parameters, 6 temporal derivatives of these parameters, and these 12 parameters squared) were used in the infant and toddler data.

Statistical Analyses

We fit five separate longitudinal mixed effects models, one model for the functional connectivity between each of the four pairs of nodes and one more model for the functional connectivity of the overall language network, defined to be the average of the functional connectivity values for the 4 pairs of nodes. To allow for flexible estimation of connectivity that could include rapid changes, for example, between the fetal and neonatal period, each model employed a piecewise linear growth curve, where different age groups were allowed to have different growth patterns as opposed to assuming constant slope or some functional form across all ages. The growth curves were taken to be continuous piecewise-linear splines that include changes in slope at specified ages referred to as knots. In addition to the growth curves, each model included sex as a fixed effect (Wheelock et al. 2019; Vasung, Rollins, Yun et al. 2020b), random effects for individuals having repeated measurements to account for the longitudinal data, and fixed effects for each cohort to allow for systematic differences across cohorts. We chose to model each cohort instead of modeling each site as to better capture the variance within the different Yale cohorts (which despite being from the same site used different sequences). For the primary analysis, results are reported for the following postmenstrual ages: 31.3 weeks (PMA31), 35.7 weeks (PMA36), 40.0 weeks (PMA40), and 44.3 weeks (PMA44).

Changes in slope of the splines were allowed at the intermediate ages PMA36 and PMA40. Linear contrasts were used to estimate and conduct hypothesis tests for mean connectivity values at those four ages and for differences in connectivity across all pairs of ages to estimate changes over time. The secondary analysis was performed in the same way with ages of interest taken to be -2 (i.e., 31.3 weeks PMA), 1, 9, 18, and 30 months.

We also investigated differences between two pairs of growth curves, specifically, the left Broca-right Broca

Table 2. Demographics for the individuals included in primary longitudinal analysis

	Yale fetal-neonatal Cohort #1	Yale fetal-neonatal Cohort #2	Total
Number	13	10	23
Number males	8 (62%)	2 (20%)	10 (44%)
Birth weight (g)	3750 +/- 670	3080 +/- 420	3460 +/- 660
PMA at birth (wks)	39.7 +/- 1.1	39.7 +/- 1.5	39.7 +/- 1.3
Number SGA (%)	1 (8%)	1 (10%)	2 (9%)
Race			
Asian	0 (0)	1 (10%)	1 (4%)
Black–African American	2 (15%)	4 (40%)	6 (26%)
Native American	0 (0%)	0 (0%)	0 (0%)
White	10 (77%)	4 (40%)	14 (61%)
More than 1 race/unknown	1 (8%)	1 (10%)	2 (9%)
Ethnicity			
Hispanic–Latinx	2 (15%)	1 (10%)	3 (13%)
PMA at scan (wks)			
Scan 1	31.4 +/- 0.7	31.1 +/- 1.2	31.3 +/- 1.0
Scan 2	35.1 +/- 0.8	35.0 +/- 0.7	35.0 +/- 0.8
Scan 3	43.4 +/- 1.3	40.6 +/- 2.4	42.5 +/- 1.8

PMA = Postmenstrual age Values are +/- SD.

connectivity compared to left Wernicke–right Wernicke connectivity, and the left Broca–left Wernicke connectivity compared to right Broca–right Wernicke connectivity. For each pair of growth curves, we subtracted for each individual and each session the corresponding functional connectivity values and fit the growth curve model described above to these differences.

Data and Code Availability

The UCLA and C-MIND datasets are available from <https://nda.nih.gov/> using dataset identifiers: NDARCOL0002026 and NDARCOL0002329, respectively. The fetal-neonatal Cohort #1 and Neonatal Cohort #2 datasets will be released on <https://nda.nih.gov/> following an embargo period. Neonatal Cohort #1 dataset is not publicly available as consent to share the data was not obtained and the cohort is lost to follow-up. Fetal-neonatal Cohort #2 is available upon request. The image analysis software (BioImage Suite) can be found at <https://medicine.yale.edu/bioimaging/suite/> and <https://bioimagesuiteweb.github.io/webapp/index.html>.

Results

Primary Longitudinal Analysis of Language Network Functional Connectivity During 30–45 Weeks PMA

Demographic Information

Demographics for the 23 individuals with longitudinal fetal-to-neonatal imaging are shown in Table 2. Ten (44%) were males, the mean birth weight was 3460 +/- 660 g and the mean PMA at birth was 39.7 +/- 1.3 weeks. Twenty-six percent were Black–African American, and 13% were of Hispanic–Latinx ethnicity.

Resting State Functional Connectivity

As shown in Table 3, the overall language network strength exceeded 0 at 45 weeks PMA. Data for the

individual connections demonstrated that both inter-hemispheric connections (i.e., left Broca’s–right Broca’s and left Wernicke’s–right Wernicke’s) exceeded 0 after birth. In contrast, the intrahemispheric connections for both left Broca’s–left Wernicke’s and right Broca’s–right Wernicke’s remained negligible during the time interval between 31- and 45-weeks PMA.

Longitudinal contrasts for the overall language network (Table 4, Fig. 1) revealed significant increases in connectivity strength across the third trimester and the perinatal transition, suggesting increases in connectivity beginning during the prenatal period and further extending into the first postnatal month.

Regarding the specific left Broca’s–right Broca’s connection, there was no significant increase over the third trimester, but significant increases were observed postnatally (Figs 2A and B and 3). For the left Wernicke’s–right Wernicke’s connection, we noted significant increases in functional connectivity for all time points compared to the beginning of the third trimester.

In contrast, no changes in connectivity strength were found in the ipsilateral Broca and Wernicke nodes either hemisphere (Fig. 2C and D). Thus, the growth pattern observed in the overall language network between 31- and 44-weeks PMA appears to be driven largely by expanding connectivity between Broca’s and Wernicke’s area and their right hemisphere homologs.

There was no difference in the growth trajectories for the two intrahemispheric connections between 31- and 44-weeks PMA (e.g., left Broca’s–left Wernicke’s connectivity compared to right Broca’s–right Wernicke’s connectivity; Table S3). Similarly, there was no difference when comparing the growth curves for the two interhemispheric connections during the same time interval (e.g., left Broca’s–right Broca’s connectivity compared to left Wernicke’s–right Wernicke’s connectivity; Table S3).

Table 3. Language network connectivity in the fetal-to-neonatal cohort at PMA 31, 35, 40, and 45 weeks

Connections	Estimate connectivity for each age			
	PMA31	PMA35	PMA40	PMA45
Overall language network	-0.12 ($P = 0.001$)	-0.16 ($P = 0.70$)	0.11 ($P = 0.06$)	0.26 ($P < 0.001$)
L Broca's-R Broca's	-0.17 ($P = 0.82$)	0.062 ($P = 0.48$)	0.34 ($P = 0.006$)	0.48 ($P = 0.008$)
L Wernicke's-R Wernicke's	-0.23 ($P = 0.003$)	-0.018 ($P = 0.83$)	0.42 ($P < 0.001$)	0.46 ($P < 0.001$)
L Broca's-L Wernicke's	-0.17 ($P = 0.03$)	-0.079 ($P = 0.38$)	-0.24 ($P = 0.06$)	0.078 ($P = 0.58$)
R Broca's-R Wernicke's	-0.073 ($P = 0.36$)	-0.023 ($P = 0.80$)	-0.11 ($P = 0.38$)	0.012 ($P = 0.93$)

PMA = Weeks postmenstrual age; P -values reflect t -test comparison of the observed connectivity strength with the value of 0.

Table 4. Change in language network connectivity in the Fetal-to-Neonatal cohort between 31, 35, 40, and 45 weeks PMA

Connections	Estimate change in connectivity between ages					
	PMA35-PMA31	PMA40-PMA35	PMA45-PMA40	PMA40-PMA31	PMA45-PMA35	PMA45-PMA31
Overall language network	0.10 ($P = 0.01$)	0.12 ($P = 0.07$)	0.15 ($P = 0.12$)	0.23 ($P < 0.001$)	0.28 ($P = 0.004$)	0.38 ($P < 0.001$)
L Broca's-R Broca's	0.080 ($P = 0.35$)	0.28 ($P = 0.06$)	0.14 ($P = 0.49$)	0.36 ($P = 0.01$)	0.42 ($P = 0.04$)	0.50 ($P = 0.01$)
L Wernicke's-R Wernicke's	0.21 ($P = 0.007$)	0.43 ($P = 0.002$)	0.039 ($P = 0.84$)	0.65 ($P < 0.001$)	0.47 ($P = 0.01$)	0.68 ($P = 0.01$)
L Broca's-L Wernicke's	0.092 ($P = 0.30$)	-0.26 ($P = 0.29$)	0.32 ($P = 0.15$)	-0.066 ($P = 0.62$)	0.16 ($P = 0.44$)	0.25 ($P = 0.21$)
R Broca's-R Wernicke's	0.050 ($P = 0.58$)	-0.087 ($P = 0.57$)	0.12 ($P = 0.58$)	-0.038 ($P = 0.79$)	0.035 ($P = 0.87$)	0.084 ($P = 0.67$)

PMA = Weeks postmenstrual age.

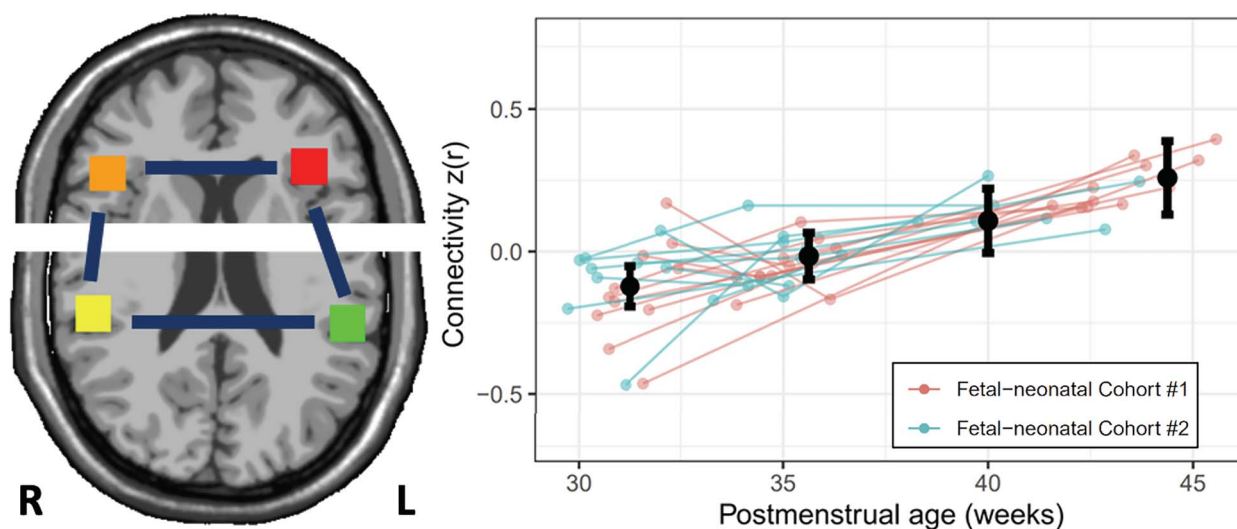


Fig. 1. Maturation of the overall language network over the third trimester and first postnatal month. A) Seeds and connections averaged together create the overall language network connectivity. As the Broca's and Wernicke's area seeds are on different axial slices, the white line in the brain indicates that two different slices are being shown in a single visualization. B) Estimates of connectivity strength at the anchors for the piecewise linear growth curve (31.3 weeks (PMA31), 35.7 weeks (PMA36), 40.0 weeks (PMA40), and 44.3 weeks (PMA44) PMA). Error bars represent 95% confident intervals. Lines indicate longitudinal data from the same participant scanned at multiple time points.

Secondary Mixed Cross-Sectional and Longitudinal Analysis of Language Network Functional Connectivity

Demographic Information

For the secondary analyses, three individuals from fetal-neonatal Cohort #1 studied at a single fetal time point at 30–32 weeks PMA (2 males) and one individual from fetal-neonatal Cohort #2 studied only at the neonatal timepoint (1 male) were included in addition to the individuals described above from these cohorts. Additionally, data from neonatal Cohort #1 ($N = 23$; 14 males), neonatal

Cohort #2 ($N = 12$; 5 males), the C-MIND study ($N = 31$; 14 males) and the UCLA NDAR data ($N = 34$; 20 males) were included. Overall, 66 of the 127 individuals were males (52%). Neonatal cohorts #1 and 2 were scanned at mean PMA of 42.9 ± 1.9 weeks (range 39–50 weeks PMA), and the racial and ethnic composition of these cohorts were like that of the infants with longitudinal scans. Individuals in the C-MIND cohort were scanned between 1 and 35 months: 8 were scanned at age < 1 year, 11 were scanned at 1–2 years, and 17 were scanned between ages 2 and 3 years. Five of the C-MIND participants

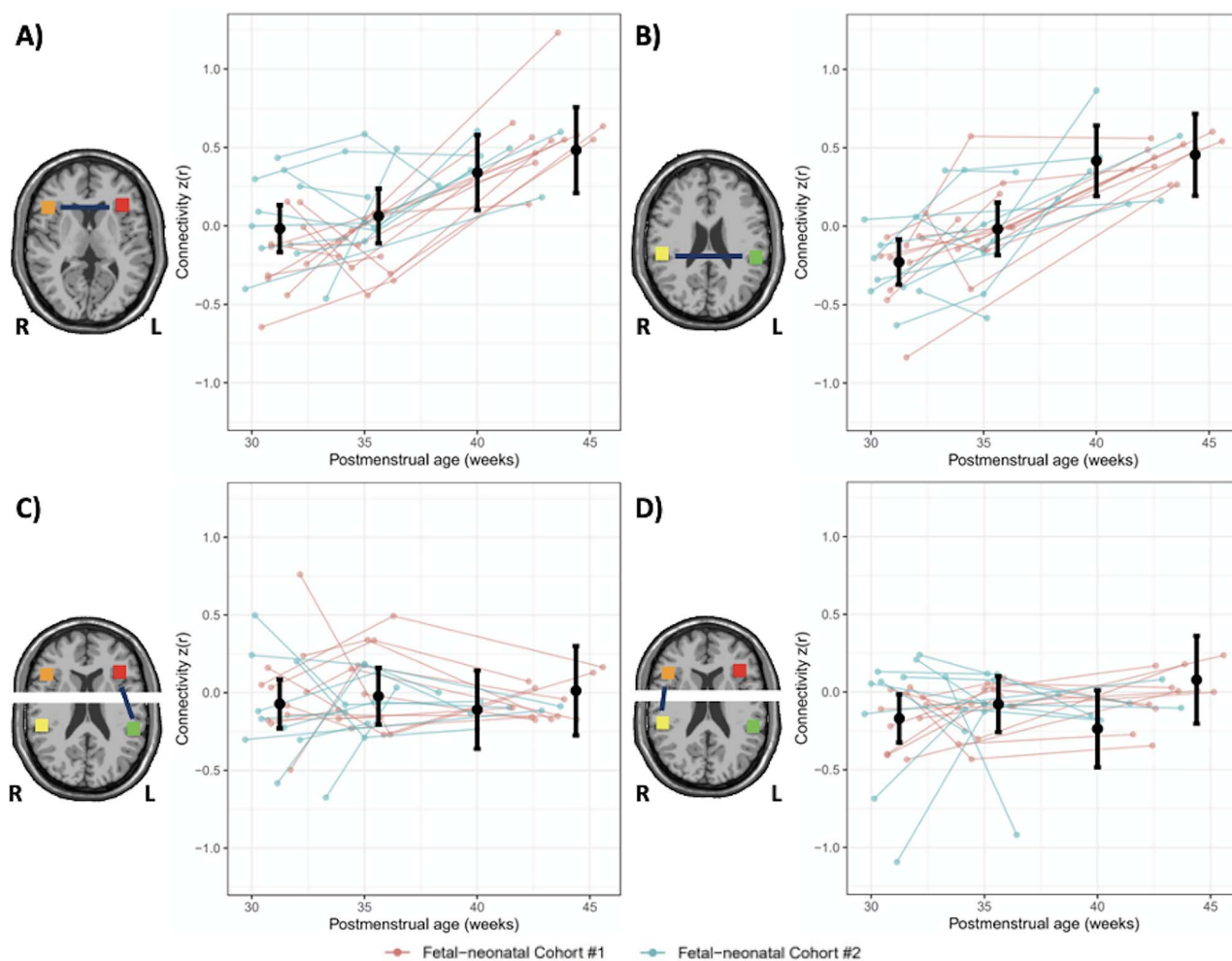


Fig. 2. Maturation of the interhemispheric and intrahemispheric language connections over the third trimester and first postnatal month. Seeds and connection used to calculate connectivity between and estimates of connectivity strength at the anchors for the piecewise linear growth curve for A) Broca's area and its right hemisphere homolog, B) Wernicke's area and its right hemisphere homolog, C) Broca's and Wernicke's area, and D) the right hemisphere homologs of Broca's and Wernicke's area. For all plots, anchors are 31.3 weeks (PMA31), 35.7 weeks (PMA36), 40.0 weeks (PMA40), and 44.3 weeks (PMA44) PMA. Error bars represent 95% confident intervals. Lines indicate longitudinal data from the same participant scanned at multiple time points. As the Broca's and Wernicke's area seeds are on different axial slices, the white line in the brain indicates that two different slices are being shown in a single visualization.

underwent longitudinal scans. For the UCLA dataset, 19 of the infants scanned at 1–2 months underwent repeat studies at 9 months of age.

Resting State Functional Connectivity

Except for the fetal period, the strength of connectivity in the overall language network was greater than zero for all ages (Table 5). Contrasts assessing longitudinal trends indicated a rapid increase in connectivity between week 31 of gestation and the first month of life. After the first month of life, language network connectivity did not significantly increase over time (Fig. 3, Table 6).

When breaking down the overall language network into its component connections, similar patterns of development were observed for interhemispheric connectivity of left Broca's area to its right hemisphere homolog and left Wernicke's area to its right hemisphere homolog. Connections between the homolog regions

were greater than 0 starting at M1 onwards (Table 5). Longitudinal analysis (Figure S1A–B) indicates increase in connectivity between the fetal period and 30 months for both homologous regions, which is driven by a rapid increase in connectivity between the fetal and neonatal periods (i.e., M1–PMA31). Changes thereafter demonstrated progressive flattening for both connections (Table 6).

In contrast to the interhemispheric connectivity, the curve for intrahemispheric connectivity between left Broca's area and left Wernicke's area (Figure S2A) demonstrated little growth across the third trimester to 30 months. No changes in nodes connectivity between 31 weeks PMA and 30 months were found. The growth curve for connectivity between right Broca's area and right Wernicke's area was similar (Figure S2B; Tables 5 and 6). Figure S3 suggests that intrahemispheric connectivity between left Broca's area and left Wernicke's area emerges between 2 and 3 years of postnatal life.

Table 5. Language network connectivity–secondary mixed cross-sectional and longitudinal analysis from 31 PMA to 30 months postnatal

Connections	Estimate connectivity for each age				
	PMA31	M1	M9	M18	M30
Overall language network	−0.084 ($P = 0.72$)	0.25 ($P < 0.001$)	0.28 ($P < 0.001$)	0.40 ($P < 0.001$)	0.34 ($P < 0.001$)
L Broca's–R Broca's	−0.0020 ($P = 0.98$)	0.45 ($P < 0.001$)	0.37 ($P < 0.001$)	0.67 ($P < 0.001$)	0.45 ($P < 0.001$)
L Wernicke's–R Wernicke's	−0.27 ($P = 0.004$)	0.45 ($P < 0.001$)	0.63 ($P < 0.001$)	0.63 ($P < 0.001$)	0.56 ($P < 0.001$)
L Broca's–L Wernicke's	−0.083 ($P = 0.32$)	0.031 ($P = 0.46$)	0.076 ($P = 0.28$)	0.12 ($P = 0.30$)	0.16 ($P = 0.19$)
R Broca's–R Wernicke's	0.0080 ($P = 0.93$)	0.058 ($P = 0.19$)	0.051 ($P = 0.44$)	0.17 ($P = 0.18$)	0.21 ($P = 0.04$)

PMA = Week postmenstrual age; M = month postnatal age; P-values reflect comparison of strength of the observed connectivity with the value of 0.

Table 6. Change in language network connectivity between ages–secondary mixed cross-sectional and longitudinal analysis

Connections	Estimate change in connectivity between ages					
	M1–PMA31	M9–M1	M18–M9	M30–M18	M30–M1	M30–PMA31
Overall language network	0.33 ($P < 0.001$)	0.031 ($P = 0.37$)	0.12 ($P = 0.08$)	−0.057 ($P = 0.25$)	0.094 ($P = 0.11$)	0.42 ($P < 0.001$)
L Broca's–R Broca's	0.45 ($P = 0.001$)	−0.079 ($P = 0.28$)	0.30 ($P = 0.04$)	−0.21 ($P = 0.05$)	0.0040 ($P = 0.97$)	0.46 ($P = 0.01$)
L Wernicke's–R Wernicke's	0.71 ($P < 0.001$)	0.12 ($P = 0.01$)	0.0070 ($P = 0.95$)	−0.072 ($P = 0.49$)	0.11 ($P = 0.35$)	0.83 ($P < 0.001$)
L Broca's–L Wernicke's	0.11 ($P = 0.32$)	0.036 ($P = 0.55$)	0.055 ($P = 0.65$)	0.0020 ($P = 0.98$)	0.094 ($P = 0.37$)	0.21 ($P = 0.18$)
R Broca's–R Wernicke's	0.051 ($P = 0.67$)	−0.0070 ($P = 0.91$)	0.12 ($P = 0.36$)	0.037 ($P = 0.70$)	0.15 ($P = 0.18$)	0.20 ($P = 0.22$)

PMA = Week gestational age; M = month postnatal age.

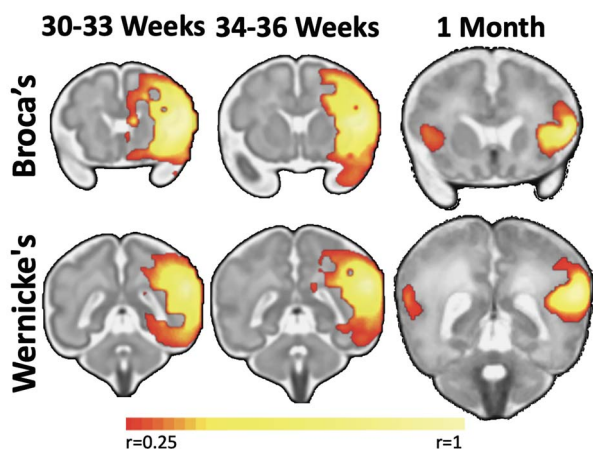


Fig. 3. Maturation of the interhemispheric connectivity for Broca's and Wernicke's area over the third trimester and first postnatal month. Seed-to-whole brain, using Broca's and Wernicke's areas as seeds, shows that interhemispheric connections between homologs were only observed for the postnatal scan.

Finally, there was no difference in the growth curves for the two intrahemispheric connections between 31 weeks of gestation through 30 months of age (e.g., left Broca's–left Wernicke's connectivity compared with right Broca's–right Wernicke's connectivity; Table S4). From 1-month to 9-months, the growth of left and right Wernicke's connectivity was significantly greater than the growth of left and right Broca's connectivity. Otherwise, there was no significance difference when comparing the growth curves for the two interhemispheric connections across the same time interval (Table S4).

Discussion

Employing longitudinal data, we demonstrate the emergence of the canonical language network from 30 weeks of gestation through 1-month postnatal age. During this critical time period, we report a significant increase in language network connectivity between the 31st and 35th weeks of gestation and an almost fourfold larger overall increase in connectivity between 31- and 45-weeks PMA. This increase is driven primarily by marked development of functional connectivity between the left and right homologs of Broca's and Wernicke's areas with the most significant changes occurring from 30 weeks of gestation through the first postnatal month. In contrast, intrahemispheric functional connectivity between left Broca's and left Wernicke's and between right Broca's and right Wernicke's showed little change during this critical time. Overall, our results show that the neural scaffolding for language begins to develop prior to birth, and functional connectivity of the language network matures rapidly in that critical period between the 31st week of gestation and the first postnatal month.

Additional data from the secondary, mixed cross-sectional and longitudinal analyses extended these growth curves into toddlerhood. Functional connectivity between the left and right homologs of Broca's and Wernicke's areas was observed for all postnatal ages with the most significant changes occurring from 31 weeks of gestation through the first postnatal month. In contrast, intrahemispheric functional connectivity between left Broca's and left Wernicke's developed slowly across this time interval with weak connectivity being detected in toddlerhood (Figure S2–S3).

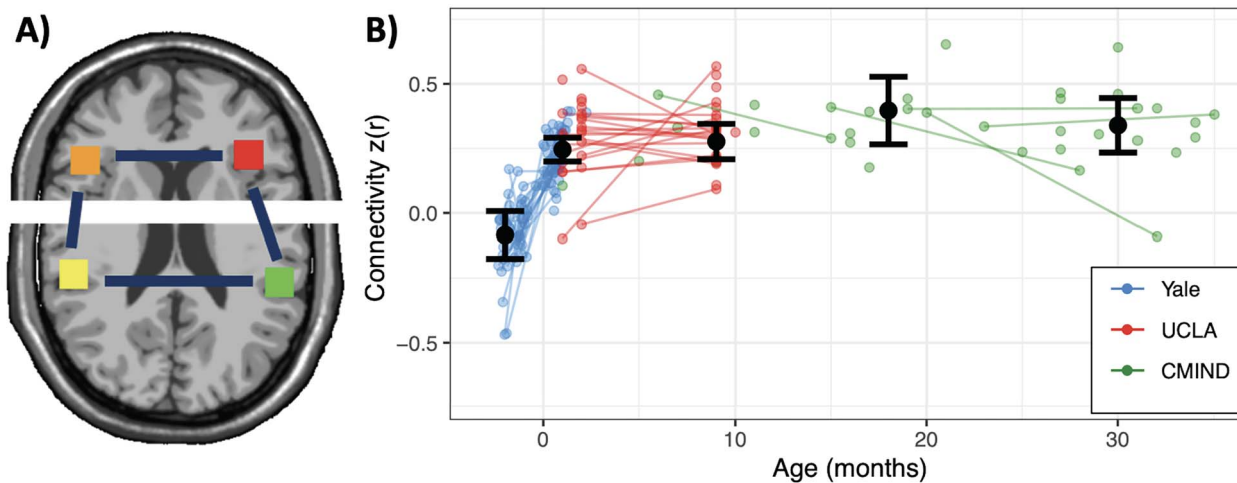


Fig. 4. Maturation of the overall language network from 30 weeks gestation to 30 months. A) Seeds and connections averaged together create the overall language network connectivity. As the Broca's and Wernicke's area seeds are on different axial slices, the white line in the brain indicates that two different slices are being shown in a single visualization. B) Estimates of connectivity strength at the anchors, -2 (i.e., 31.3 weeks PMA), 1, 9, 18, and 30 months, for the piecewise linear growth curve. Error bars represent 95% confident intervals. Lines indicate longitudinal data from the same participant scanned at multiple time points.

Broadly, our results—that interhemispheric connectivity develops across the third trimester and intra-hemispheric connectivity develops later—are consistent with previous studies of the development of Broca's and Wernicke's area functional connectivity (Perani et al. 2011; Thomason et al. 2013; Thomason et al. 2014; Kwon et al. 2015; Emerson et al. 2016; Eyre et al. 2021). Critically, these previous studies focused solely on prenatal development or postnatal development of Broca's and Wernicke's connectivity—thus missing critical information from the perinatal transition. Yet, by including longitudinal scanning from the third trimester through the first postnatal month combined with additional data through toddlerhood, we uniquely show that these interhemispheric connections exhibit connection strengths similar to older toddlers by birth during this period. We found that rate of increase of interhemispheric connectivity of the Wernicke's homologs was significantly greater than that of the Broca's homologs from 1 month to 9 months of age. This result can be broadly view in alignment with neuropathologic data and microstructural imaging data as well as studies suggesting that receptive language precedes expressive language (Huttenlocher and Dabholkar 1997; Lebenberg et al. 2019) (Fig. 4).

Function parallels structure. As neural connections on a microstructural level are formed, functional connectivity is detected in developing brain (Vasung et al. 2019). Emerging fetal diffusion tensor imaging studies suggest the possibility of tracking microstructural connectivity across the third trimester of gestation (Lockwood Estrin et al. 2019; Hunt et al. 2020; Jaimes et al. 2020). Although none of the recent publications specifically target the language system, work by Jaimes et al. demonstrates significant increases in both volume and fractional anisotropy of the uncinate fasciculus across the third

trimester of gestation (Jaimes et al. 2020). Additionally, studies document the presence of structural connectivity between Broca's and Wernicke's areas in neonates at 1–3 days of age (Brauer et al. 2013). Finally, anatomical MRI studies highlight structural asymmetries present in the developing language system in preterm infants prior to their due dates (Dubois et al. 2010). Together with our results, these suggest that structural changes for Broca's and Wernicke's areas may precede observed functional connectivity changes. Nevertheless, given that language itself emerges only in later infancy and toddlerhood, it is possible that the earlier structural development is not sufficient for language and merely lays the foundation for later functional changes.

Task-based fMRI studies in infants reveal both bilateral and left-lateralized patterns of activation in Broca's and Wernicke's regions (Dehaene-Lambertz et al. 2002; Perani et al. 2011; Shultz et al. 2014). Broca's and Wernicke's regions activate to language-based stimuli, show expected lateralization patterns in the left hemisphere, and demonstrate activation patterns resembling those in older children and even adults during the first weeks of life (Dehaene-Lambertz et al. 2002; Dehaene-Lambertz et al. 2006; Perani et al. 2011). Thus, although speech activates language regions and homologs are connected in infancy, Broca's and Wernicke's areas in the same hemisphere remain poorly functionally connected in infancy. Overall, the functional systems for language in infants appear be more bilaterally organized than those in school-age children, adolescents, and adults.

Emerging data suggest the impact of genetic and environmental factors on the development of language systems. Resting state functional connectivity in a left hemisphere pre-language region is decreased in fetuses three weeks before they are born preterm

(Thomason et al. 2017), neural networks for language are altered at birth prior to the hypoxemia that may accompany major surgery in infants with complex congenital heart disease (De Asis-Cruz et al. 2018), and infants later diagnosed with ASD show altered functional connectivity long before they develop symptoms of this disorder (Emerson et al. 2017; Rolison et al. 2021). In addition, antenatal maternal anxiety exposure decreases fetal functional connectivity (De Asis-Cruz et al. 2020). Infants who receive breast milk show greater microstructural connectivity (Deoni et al. 2013; Blesa et al. 2019). The neural correlates of human fetal learning of speech-like auditory stimuli have been demonstrated (Partanen et al. 2013). As language is critical for later cognition (Goldin-Meadow et al. 2014), the trajectory of the neural systems for language—similar to the ones observed here—must be defined first. These systems provide a platform to study developmental disorders associated with aberrant language abilities in fetuses, infants, and toddlers and may provide insight into circuits to be targeted for early interventions.

The strengths of our study include longitudinal imaging across the pre- and postnatal periods. By including fetal-to-neonatal scanning along with imaging in later infancy and toddlerhood, we uniquely demonstrate that the strength of interhemispheric connectivity of the language network mainly develops during the third trimester. Other strengths of this work include the high number of participants, many with longitudinal imaging, and the statistical analysis strategies. In addition, to the best of our knowledge, this is the first study to provide longitudinal functional connectivity for fetuses-to-neonates across the third trimester of gestation, perinatal transition and during the first postnatal month. We used an open-science approach to pool multiple smaller samples together to increase both the number of data points and the age range of participants following the neonatal period (Costafreda 2009). While an ideal case is to have longitudinal data from the fetal period through toddlerhood, these studies are often prohibitive for a single study, and merging independent data from diverse samples is a powerful and needed alternative. Finally, the relative size of cortical regions has been reported to be conserved and determined early during development, although there are more subtle growth differences between regions during periods of peak thalamocortical growth (Vasung, Rollins, Velasco-Annis et al. 2020a), and we employed age-appropriate fetal templates. To address this issue, we used piecewise linear growth curves, where age groups are allowed to have different growth patterns, to map development trajectories. As opposed to making the hard assumption of a single growth function across all ages, this approach allows the data to “speak for itself” and naturally captures periods of rapid change.

The limitations of fetal functional imaging have been well described (Thomason et al. 2017; Thomason 2020) and range from variations in fetal brain orientation, motion, the influence of placental, maternal and fetal

physiological signals and the very small head size to changes in fetal cerebral metabolism and the limited understanding of the physiologic basis of the BOLD fMRI signals in fetal brain. As reviewed by Thomason, these are persisting concerns for MRI studies in neonates and young children, and we have used many of the previously published strategies to address these concerns (Glover et al. 2000; Power et al. 2012; Avants et al. 2014; Scheinost et al. 2018; Rutherford et al. 2021). In addition, as noted above, we used gestational age-appropriate fetal templates to address the significant growth in fetal brain across the third trimester of gestation.

Cerebral metabolism increases across the third trimester of gestation, but the characterization of the neurovascular coupling, or the “neural activation support mechanism involving synergistic interactions between the metabolic and vascular systems” (Govindan et al. 2016), has not yet been reported in the fetal brain. Although, preclinical and human studies suggest the presence of neurovascular coupling across the third trimester of gestation (Logothetis et al. 2001; Chalak et al. 2017; Chalak and Zhang 2017; Mahmoudzadeh et al. 2018; Das et al. 2020; Hendrikx et al. 2020). Finally, our data are consistent with neuroanatomic and both functional and structural fetal data suggesting the emergence of long-range functional connections followed by intrahemispheric ones (Dubois et al. 2009; Huang et al. 2009; Leroy et al. 2011; Dubois et al. 2014; Cohen et al. 2016; Wang et al. 2017; Wilkinson et al. 2017; Lebenberg et al. 2019; Jaimes et al. 2020).

Employing longitudinal data, we show the developmental trajectories of functional connectivity within the language network from 30 weeks of gestation through 1-month postnatal age. Together, these results suggest that the functional connectivity for language begins to develop prior to birth. Future studies should continue to map these trajectories with increased sampling in the late third trimester, investigate the impact of genetic and environmental factors on these data, and develop early interventions aimed at targeting the abnormal circuits these trajectories identify.

Supplementary Material

Supplementary material can be found at *Cerebral Cortex* online.

Funding

P50HD093078 from the National Institutes of Health.

Notes

We are grateful to Hedy Sarofin, RTR, MR, ARRT, the ACE research fellows Hannah Feiner BS, Rachel Foster BS, Hannah Neiderman BA, and Carolyn Gershman BA for technical assistance, Sahand Negahban, PhD and the ACE Statistics Core for their input on statistical analysis, Kelly Powell PhD, Suzanne Macari PhD, Katherine Kohari MD,

Soo Kwon MD, Chelsea Morgan PsyD, James McPartland PhD and Fred Volkmar MD, and Amy Giguere Carney, MSW for their contribution to sample recruitment and characterization. The authors thank the families for their participation. *Conflict of Interest:* The authors declare no competing financial interests.

References

- Avants BB, Tustison NJ, Stauffer M, Song G, Wu B, Gee JC. 2014. The Insight ToolKit image registration framework. *Front Neuroinform.* 8:44.
- Blesa M, Sullivan G, Anblagan D, Telford EJ, Quigley AJ, Sparrow SA, Serag A, Semple SI, Bastin ME, Boardman JP. 2019. Early breast milk exposure modifies brain connectivity in preterm infants. *Neuroimage.* 184:431–439.
- Brauer J, Anwander A, Perani D, Friederici AD. 2013. Dorsal and ventral pathways in language development. *Brain Lang.* 127: 289–295.
- Bruchhage MMK, Ngo GC, Schneider N, D'Sa V, Deoni SCL. 2020. Functional connectivity correlates of infant and early childhood cognitive development. *Brain Struct Funct.* 225:669–681.
- Chalak LF, Tian F, Adams-Huet B, Vasil D, Laptook A, Tarumi T, Zhang R. 2017. Novel wavelet real time analysis of neurovascular coupling in neonatal encephalopathy. *Sci Rep.* 7:45958.
- Chalak LF, Zhang R. 2017. New wavelet neurovascular bundle for bedside evaluation of cerebral autoregulation and neurovascular coupling in newborns with hypoxic-ischemic encephalopathy. *Dev Neurosci.* 39:89–96.
- Cohen AH, Wang R, Wilkinson M, MacDonald P, Lim AR, Takahashi E. 2016. Development of human white matter fiber pathways: from newborn to adult ages. *Int J Dev Neurosci.* 50:26–38.
- Costafreda SG. 2009. Pooling fMRI data: meta-analysis, mega-analysis and multi-center studies. *Front Neuroinform.* 3:33.
- Das Y, Liu H, Tian F, Kota S, Zhang R, Chalak LF. 2020. Rigor of neurovascular coupling (NVC) assessment in newborns using different amplitude EEG algorithms. *Sci Rep.* 10:9183.
- De Asis-Cruz J, Donofrio MT, Vezina G, Limperopoulos C. 2018. Aberrant brain functional connectivity in newborns with congenital heart disease before cardiac surgery. *Neuroimage Clin.* 17:31–42.
- De Asis-Cruz J, Krishnamurthy D, Zhao L, Kapse K, Vezina G, Andescavage N, Quistorff J, Lopez C, Limperopoulos C. 2020. Association of prenatal maternal anxiety with fetal regional brain connectivity. *JAMA Netw Open.* 3:e2022349.
- Dehaene-Lambertz G, Dehaene S, Hertz-Pannier L. 2002. Functional neuroimaging of speech perception in infants. *Science.* 298: 2013–2015.
- Dehaene-Lambertz G, Hertz-Pannier L, Dubois J, Meriaux S, Roche A, Sigman M, Dehaene S. 2006. Functional organization of perisylvian activation during presentation of sentences in preverbal infants. *Proc Natl Acad Sci U S A.* 103:14240–14245.
- Deoni SC, Dean DC, Piryatinsky I, O'Muircheartaigh J, Waskiewicz N, Lehman K, Han M, Dirks H. 2013. Breastfeeding and early white matter development: a cross-sectional study. *Neuroimage.* 82:77–86.
- Dubois J, Benders M, Lazeyras F, Borradori-Tolsa C, Leuchter RH, Mangin JF, Huppi PS. 2010. Structural asymmetries of perisylvian regions in the preterm newborn. *Neuroimage.* 52:32–42.
- Dubois J, Dehaene-Lambertz G, Kulikova S, Poupon C, Huppi PS, Hertz-Pannier L. 2014. The early development of brain white matter: a review of imaging studies in fetuses, newborns and infants. *Neuroscience.* 276:48–71.
- Dubois J, Hertz-Pannier L, Cachia A, Mangin JF, Le Bihan D, Dehaene-Lambertz G. 2009. Structural asymmetries in the infant language and sensori-motor networks. *Cereb Cortex.* 19:414–423.
- Emerson RW, Adams C, Nishino T, Hazlett HC, Wolff JJ, Zwaigenbaum L, Constantino JN, Shen MD, Swanson MR, Elison JT, et al. 2017. Functional neuroimaging of high-risk 6-month-old infants predicts a diagnosis of autism at 24 months of age. *Sci Transl Med.* 9.
- Emerson RW, Gao W, Lin W. 2016. Longitudinal study of the emerging functional connectivity asymmetry of primary language regions during infancy. *J Neurosci.* 36(42):10883–10892.
- Eyre M, Fitzgibbon SP, Ciarrusta J, Cordero-Grande L, Price AN, Poppe T, Schuh A, Hughes E, O'Keefe C, Brandon J, et al. 2021. The Developing Human Connectome Project: typical and disrupted perinatal functional connectivity. *Brain.* 144(7):2199–2213.
- Gholipour A, Rollins CK, Velasco-Annis C, Ouaalam A, Akhondi-Asl A, Afacan O, Ortinau CM, Clancy S, Limperopoulos C, Yang E, et al. 2017. A normative spatiotemporal MRI atlas of the fetal brain for automatic segmentation and analysis of early brain growth. *Sci Rep.* 7:476.
- Glover GH, Li TQ, Ress D. 2000. Image-based method for retrospective correction of physiological motion effects in fMRI: RETROICOR. *Magn Reson Med.* 44:162–167.
- Goldin-Meadow S, Levine SC, Hedges LV, Huttenlocher J, Raudenbush SW, Small SL. 2014. New evidence about language and cognitive development based on a longitudinal study: hypotheses for intervention. *Am Psychol.* 69:588–599.
- Govindan RB, Massaro A, Chang T, Vezina G, du Plessis A. 2016. A novel technique for quantitative bedside monitoring of neurovascular coupling. *J Neurosci Methods.* 259:135–142.
- Hendrikx D, Thewissen L, Smits A, Naulaers G, Allegaert K, Van Huffel S, Caicedo A. 2020. Nonlinear transfer entropy to assess the neurovascular coupling in premature neonates. *Adv Exp Med Biol.* 1232:11–17.
- Huang H, Xue R, Zhang J, Ren T, Richards LJ, Yarowsky P, Miller MI, Mori S. 2009. Anatomical characterization of human fetal brain development with diffusion tensor magnetic resonance imaging. *J Neurosci.* 29:4263–4273.
- Hunt D, Dighe M, Gatenby C, Studholme C. 2020. Automatic, age consistent reconstruction of the corpus callosum guided by coherency from in utero diffusion-weighted MRI. *IEEE Trans Med Imaging.* 39:601–610.
- Huttenlocher P, Dabholkar A. 1997. Regional differences in synaptogenesis in human cerebral cortex. *J Comp Neurol.* 387:167–178.
- Jaimes C, Machado-Rivas F, Afacan O, Khan S, Marami B, Ortinau CM, Rollins CK, Velasco-Annis C, Warfield SK, Gholipour A. 2020. In vivo characterization of emerging white matter microstructure in the fetal brain in the third trimester. *Hum Brain Mapp.* 41: 3177–3185.
- Jardri R, Houfflin-Debarge V, Delion P, Pruvo JP, Thomas P, Pins D. 2012. Assessing fetal response to maternal speech using a noninvasive functional brain imaging technique. *Int J Dev Neurosci.* 30: 159–161.
- Joshi A, Scheinost D, Okuda H, Belhachemi D, Murphy I, Staib LH, Papademetris X. 2011. Unified framework for development, deployment and robust testing of neuroimaging algorithms. *Neuroinformatics.* 9:69–84.
- Kwon SH, Scheinost D, Lacadie C, Benjamin J, Myers EH, Qiu M, Schneider KC, Rothman DL, Constable RT, Ment LR. 2014. GABA, resting-state connectivity and the developing brain. *Neonatology.* 106:149–155.
- Kwon SH, Scheinost D, Lacadie C, Sze G, Schneider KC, Dai F, Constable RT, Ment LR. 2015. Adaptive mechanisms of developing brain:

- cerebral lateralization in the prematurely-born. *Neuroimage*. 108: 144–150.
- Lebenberg J, Mangin JF, Thirion B, Poupon C, Hertz-Pannier L, Leroy F, Adibpour P, Dehaene-Lambertz G, Dubois J. 2019. Mapping the asynchrony of cortical maturation in the infant brain: an MRI multi-parametric clustering approach. *Neuroimage*. 185:641–653.
- Leroy F, Glasel H, Dubois J, Hertz-Pannier L, Thirion B, Mangin JF, Dehaene-Lambertz G. 2011. Early maturation of the linguistic dorsal pathway in human infants. *J Neurosci*. 31:1500–1506.
- Lockwood Estrin G, Wu Z, Deprez M, Bertelsen A, Rutherford MA, Counsell SJ, Hajnal JV. 2019. White and grey matter development in utero assessed using motion-corrected diffusion tensor imaging and its comparison to ex utero measures. *MAGMA*. 32: 473–485.
- Logothetis NK, Pauls J, Augath M, Trinath T, Oeltermann A. 2001. Neurophysiological investigation of the basis of the fMRI signal. *Nature*. 412:150–157.
- Mahmoudzadeh M, Dehaene-Lambertz G, Kongolo G, Fournier M, Goudjil S, Wallois F. 2018. Consequence of intraventricular hemorrhage on neurovascular coupling evoked by speech syllables in preterm neonates. *Dev Cogn Neurosci*. 30:60–69.
- Morton SU, Brodsky D. 2016. Fetal physiology and the transition to extrauterine life. *Clin Perinatol*. 43:395–407.
- Partanen E, Kujala T, Naatanen R, Liitola A, Sambeth A, Huotilainen M. 2013. Learning-induced neural plasticity of speech processing before birth. *Proc Natl Acad Sci U S A*. 110:15145–15150.
- Perani D, Saccuman MC, Scifo P, Anwander A, Spada D, Baldoli C, Poloniato A, Lohmann G, Friederici AD. 2011. Neural language networks at birth. *Proc Natl Acad Sci U S A*. 108:16056–16061.
- Peyvandi S, Xu D, Wang Y, Hogan W, Moon-Grady A, Barkovich AJ, Glenn O, McQuillen P, Liu J. 2021. Fetal cerebral oxygenation is impaired in congenital heart disease and shows variable response to maternal hyperoxia. *J Am Heart Assoc*. 10(1):e018777.
- Power JD, Barnes KA, Snyder AZ, Schlaggar BL, Petersen SE. 2012. Spurious but systematic correlations in functional connectivity MRI networks arise from subject motion. *Neuroimage*. 59:2142–2154.
- Rolison M, Lacadie C, Chawarska K, Spann M, Scheinost D. 2021. Atypical intrinsic hemispheric interaction associated with autism spectrum disorder is present within the first year of life. *Cereb Cortex*. bhab284. <https://doi.org/10.1093/cercor/bhab284>.
- Rutherford S, Sturmfels P, Angstadt M, Hect J, Wiens J, van den Heuvel MI, Scheinost D, Sripatha C, Thomason M. 2021. Automated Brain Masking of Fetal Functional MRI with Open Data. *Neuroinformatics*. <https://doi.org/10.1007/s12021-021-09528-5>.
- Scheinost D, Kwon SH, Lacadie C, Sze G, Sinha R, Constable RT, Ment LR. 2016a. Prenatal stress alters amygdala functional connectivity in preterm neonates. *Neuroimage Clin*. 12:381–388.
- Scheinost D, Kwon SH, Lacadie C, Vohr BR, Schneider KC, Papademetris X, Constable RT, Ment LR. 2017. Alterations in anatomical covariance in the prematurely born. *Cerebral Cortex*. 27:534–543.
- Scheinost D, Kwon SH, Shen X, Lacadie C, Schneider KC, Dai F, Ment LR, Constable RT. 2016b. Preterm birth alters neonatal, functional rich club organization. *Brain Struct Funct*. 221:3211–3222.
- Scheinost D, Onofrey JA, Kwon SH, Cross SN, Sze G, ML R, Papademetris X. 2018 4-7 April 2018. A fetal fMRI specific motion correction algorithm using 2nd order edge features. In: 2018 IEEE 15th International Symposium on Biomedical Imaging (ISBI 2018). Piscataway, NJ: IEEE, pp. 1288–1292.
- Scheinost D, Papademetris X, Constable RT. 2014. The impact of image smoothness on intrinsic functional connectivity and head motion confounds. *Neuroimage*. 95:13–21.
- Schwaberg B, Pichler G, Binder-Heschl C, Baik-Schneditz N, Avian A, Urlesberger B. 2018. Cerebral blood volume during neonatal transition in term and preterm infants with and without respiratory support. *Front Pediatr*. 6:132.
- Shultz S, Vouloumanos A, Bennett RH, Pelphrey K. 2014. Neural specialization for speech in the first months of life. *Dev Sci*. 17: 766–774.
- Sobell LC, Sobell MB. 1995. *Alcohol Timeline Followback Users' Manual*. Toronto, CAN: Addictin Research Foundation.
- Thomason ME. 2020. Development of brain networks in utero: relevance for common neural disorders. *Biol Psychiatry*. 88: 40–50.
- Thomason ME, Brown JA, Dassanayake MT, Shastri R, Marusak HA, Hernandez-Andrade E, Yeo L, Mody S, Berman S, Hassan SS, et al. 2014. Intrinsic functional brain architecture derived from graph theoretical analysis in the human fetus. *PLoS One*. 9(5): e94423.
- Thomason ME, Dassanayake MT, Shen S, Katkuri Y, Alexis M, Anderson AL, Yeo L, Mody S, Hernandez-Andrade E, Hassan SS, et al. 2013. Cross-hemispheric functional connectivity in the human fetal brain. *Sci Transl Med*. 5(173):173ra124.
- Thomason ME, Scheinost D, Manning JH, Grove LE, Hect J, Marshall N, Hernandez-Andrade E, Berman S, Pappas A, Yeo L, et al. 2017. Weak functional connectivity in the human fetal brain prior to preterm birth. *Sci Rep*. 7:39286.
- Tomasi D, Volkow ND. 2012. Language network: segregation, laterality and connectivity. *Mol Psychiatry*. 17:759.
- Turk E, van den Heuvel MI, Benders MJ, de Heus R, Franx A, Manning JH, Hect JL, Hernandez-Andrade E, Hassan SS, Romero R, et al. 2019. Functional connectome of the fetal brain. *J Neurosci*. 39: 9716–9724.
- Vasung L, Abaci Turk E, Ferradal SL, Sutin J, Stout JN, Ahtam B, Lin PY, Grant PE. 2019. Exploring early human brain development with structural and physiological neuroimaging. *Neuroimage*. 187: 226–254.
- Vasung L, Rollins CK, Velasco-Annis C, Yun HJ, Zhang J, Warfield SK, Feldman HA, Gholipour A, Grant PE. 2020a. Spatiotemporal differences in the regional cortical plate and subplate volume growth during fetal development. *Cereb Cortex*. 30: 4438–4453.
- Vasung L, Rollins CK, Yun HJ, Velasco-Annis C, Zhang J, Wagstyl K, Evans A, Warfield SK, Feldman HA, Grant PE, et al. 2020b. Quantitative in vivo MRI assessment of structural asymmetries and sexual dimorphism of transient fetal compartments in the human brain. *Cereb Cortex*. 30:1752–1767.
- Wang R, Wilkinson M, Kane T, Takahashi E. 2017. Convergence of cortical, thalamocortical, and callosal pathways during human fetal development revealed by diffusion MRI tractography. *Front Neurosci*. 11:576.
- Weinberger AH, Reutenauer EL, Allen TM, Termine A, Vessicchio JC, Sacco KA, Easton CJ, McKee SA, George TP. 2007. Reliability of the fagerstrom test for nicotine dependence, minnesota nicotine withdrawal scale, and tiffany questionnaire for smoking urges in smokers with and without schizophrenia. *Drug Alcohol Depend*. 86: 278–282.
- Wheelock MD, Hect JL, Hernandez-Andrade E, Hassan SS, Romero R, Eggebrecht AT, Thomason ME. 2019. Sex differences in functional connectivity during fetal brain development. *Dev Cogn Neurosci*. 36:100632.
- Wilkinson M, Lim AR, Cohen AH, Galaburda AM, Takahashi E. 2017. Detection and growth pattern of arcuate fasciculus from newborn to adult. *Front Neurosci*. 11:389.